
Article:
Ramírez-González, J. and West, A.R. (2021) Electrical properties of Mg-doped and Mg, Si co-doped alumina. Journal of the European Ceramic Society, 41 (6). pp. 3512-3519. ISSN: 0955-2219

https://doi.org/10.1016/j.jeurceramsoc.2020.12.040

Electrical properties of Mg-doped and Mg, Si co-doped alumina

Julia Ramírez-González and Anthony R. West

Department of Materials Science and Engineering, The University of Sheffield, Mappin Street, Sheffield S1 3JD, UK

Abstract

Impedance measurements on Mg-doped alumina ceramics, over the temperature range 400-910 °C, showed a combination of oxide ion conductivity and p-type electronic conductivity, depending on temperature and oxygen partial pressure. The oxide ion conductivity is attributed to oxygen vacancies, introduced as charge compensation for the Mg dopant. The p-type conductivity is attributed to hole creation on under-bonded oxide ions and is the dominant conductivity for measurements in air at high temperatures. In samples co-doped with Mg and Si, impedance measurements showed a reduction in oxide ion conductivity and therefore, number of oxide ion vacancies because the self-compensation mechanism of co-doping lead to direct replacement of Al^{3+} by Mg^{2+} and Si^{4+}; the level of p-type conductivity was also reduced.

Keywords: alumina, impedance spectroscopy, p-type conductivity, oxide ion conductivity

1.Introduction

The defect structure and electrical properties of pure and doped Al_2O_3 have been the focus of many studies since 1960 [1]. Extensive reviews on the diffusion of oxygen and aluminium have been written [2][3][4] which reflect the continuing debate and unresolved questions on this topic.

The defects responsible for conductivity and/or diffusion were considered variously to be aluminium vacancies ($V_{Al}^{'''}$), aluminium interstitials ($Al_i^{\bullet\bullet\bullet}$), oxygen vacancies ($V_O^{\bullet\bullet}$) and oxygen interstitials ($O_i^{''}$) [5]–[17]. These were suggested from a wide range of diffusion experiments, *dc* and *ac* conductivity measurements, consideration of the thermodynamics of defect equilibria including the energetics of formation of Schottky and Frenkel defects, molecular dynamic and atomic scale simulations. Difficulties in identifying the intrinsic defects in alumina arise from the similarity in formation energies of oxygen Frenkel and Schottky defects [16], [17] and their sensitivity to impurities: a few ppm may create defects whose consequences overshadow the effects of intrinsic defect concentrations [17].

Studies involving a wide range of dopants suggested that divalent ions are compensated by $V_O^{\bullet\bullet}$ and tetravalent ions by $V_{Al}^{'''}$ [7], [16]. However, it was also suggested that if Frenkel defects predominate, divalent cations are compensated by $Al_i^{\bullet\bullet\bullet}$ [7] and $O_i^{''}$ species compensate for the dissolution of Ti^{4+}, rather than $V_{Al}^{'''}$[15]. There is general agreement that oxygen diffusion increases with Mg-doping and decreases with Ti-doping; it was concluded that oxygen diffusion occurs via $V_O^{\bullet\bullet}$ in the former and $O_i^{''}$ in the latter and that $V_O^{\bullet\bullet}$ diffusion is 2-2.5 times faster than that of $O_i^{''}$ [2]. Nevertheless, aluminium diffusion, as either vacancies or interstitials, was also considered possible, with the conclusion that $Al_i^{\bullet\bullet\bullet}$ dominates in the presence of Mg^{2+} and $V_{Al}^{'''}$ in the presence of Ti^{4+} [2]. When comparing aluminium and oxygen diffusion, $Al_i^{\bullet\bullet\bullet}$ diffuses 10^3-10^4 times faster than $V_O^{\bullet\bullet}$ [2] and the presence of Si increases the amount of $V_{Al}^{'''}$ [12].

Conductivity measurements at 1650°C showed a large variation with pO_2. The electronic conductivity increased in either reducing or oxidizing atmospheres and was separated by an electrolytic domain that became increasingly broadened as temperature decreased to 1200°C [11]. Due to the resistive nature of the material, long times were necessary to reach equilibrium below 1200°C [12]. Depending on stoichiometry and experimental conditions, especially temperature and oxygen partial pressure, pO_2, Al_2O_3 could present both electronic (*n*- or *p*-type) and/or ionic conductivity. Consistent with this observation, thermoelectric emf experiments showed that the hot junction on a single crystal

of Al_2O_3 was positive under pure oxygen and negative under low pO_2 (~10^{-10} atm) [5]. Other factors to be considered in rationalising knowledge of defect concentrations and equilibria with conductivity and diffusion data include the distinction between continuous, long range conduction and short range hops over barriers that have the lowest energy, the possibility of defect-defect interactions and the formation of charged or neutral clusters; these appear to be ignored in most cases [4].

Alumina-based ceramics have found use in a wide range of commercial applications due to their many key properties. Exceptionally high electrical resistivity, high mechanical strength, corrosion resistance and thermal stability well above 1000 °C, as well as biological inertness, combine to allow extensive utilisation of Al_2O_3.[18] The cost of manufacturing Al_2O_3 ceramic components is highly dependent on the purity and processing routes used, which in turn influence the microstructure and final properties. A balance in both cost and final properties must be reached depending on the final application. For example, a small grain size (< 2 μm) and high purity (> 99 %) are desired in demanding mechanical and chemically corrosive applications, but can be costly. There is also a necessity for the addition of a sintering aid, commonly MgO, which enables the Al_2O_3 ceramic to sinter to near full density, whilst controlling grain growth [19], [20].

Often, a secondary glass phase is used as a processing aid, despite potentially lowering the ceramic's mechanical strength. As an electrical insulator, Al_2O_3 ceramics can benefit from a glass phase through improved bonding strength to metallisation inks used for metal assemblies. The use of a glassy secondary phase also aids sintering, with rates of mass transport increased at relatively lower firing temperatures, allowing for the use of a larger starting particle size Al_2O_3, reducing the overall cost of production [21]. For electrically insulating applications, such as electrical feedthrough or high voltage power tubes, it is important that the addition of a sintering aid does not diminish the electrical resistivity of the Al_2O_3. Understanding the electrical resistance behaviour of an Al_2O_3 ceramic can aid in understanding why some grades perform better in specific applications, whilst directing the future development of new grades.

The main purpose of this study has been to use impedance spectroscopy to measure the electrical properties of doped alumina ceramics at much lower temperatures, ~ 500-900 ^oC, than those used to evaluate defect equilibria, usually in single crystal materials, at very high temperatures, > ~ 1400 ^oC. The objective is to identify and understand the main factors and principal defects that control the conductivity of doped ceramics, whether ionic or electronic. Although the materials are unlikely to be in thermodynamic equilibrium with the atmosphere at these relatively low temperatures, the properties should nevertheless be dominated by the defects and their concentrations that have been frozen in from higher temperatures. The materials may, therefore, exhibit kinetic stability and associated metastable equilibria that have a controlling effect on electrical properties at lower temperatures. Two types of Mg-doped alumina ceramics have been studied, both with and without the addition of silica. It was of interest to see whether the addition of silica led to the presence of a separate glassy phase or whether it could dissolve in the alumina lattice. The results demonstrate particularly well the sensitivity of electrical conductivity to the charge compensation mechanism associated with aliovalent dopants.

2.Experimental

Samples of composition: 0.05wt%MgO-Al_2O_3 (Mg0.05) and 0.5wt%(MgO/SiO_2)-Al_2O_3, with a Mg:Si ratio of 1:6 (Mg0.5) were analysed. These compositions were prepared from reagent grade (> 99%) Al_2O_3 (Almatis), $Mg(NO_3)_2{\cdot}4H_2O$ (Sigma Aldrich) and $Si(OC_2H_5)_4$ (Sigma Aldrich). The reagents were combined with inorganic additives and organic binders and mixed in an aqueous slurry before spray

drying. Dried powders were pressed uniaxially in air using a 20 mm pellet die at 150 MPa before debinding and sintering at typically 1550°C for 8 h in air. The final fired density of the pellets was 3.94 and 3.86 g/cm^3 for Mg0.05 and Mg0.5, respectively.

Sintered samples were polished metallographically, thermally etched at 1350°C for 20 min and sputter-coated with 10 nm of carbon. Ceramic microstructures were determined by secondary electron (SE) images taken on a field-emission scanning electron microscope (FEI Inspect F50) using an acceleration voltage of 15 kV and energy-dispersion analysis of x-rays (EDS) from Oxford Instruments using 20 kV.

For impedance measurements, Pt paste electrodes were applied to opposite pellet faces and dried at 900°C for 2 h. Electroded pellets were attached to the Pt leads of a conductivity jig which allowed the flow of gas. Isothermal impedance measurements were taken after 30 min of flowing N_2, O_2 and dried air at 101.325 kPa, over the temperature range 400-950 °C. Two impedance analysers were used: a Solartron SI 1260 (measurement accuracy ±0.1%), frequency range 10 mHz-1 MHz and an Agilent Agilent 4294A (measurement accuracy ±0.08%), frequency range 40 Hz-1 MHz, with a nominal *ac* voltage of 100 mV in both cases.

Two sets of corrections were made to the collected data: (i) a geometric factor consisting of pellet thickness and sample-electrode contact area and (ii) jig impedance characteristics consisting of the blank, open circuit capacitance, typically 6 pF and the closed circuit resistance of, primarily, the leads, 1-2 Ω. The reported values for bulk resistances, R_1, correspond approximately to their resistivities; grain boundary resistances, R_2, are not resistivities as they were not corrected for grain boundary geometries, although they are reported also in units of ohm cm. Data analysis was performed using ZVIEW software (ZVIEW-Impedance Software version 2.4 Scribner Associates).

3.Results

Mg0.05 gave a typical impedance complex plane response characterised by 3 electrical components, Figure 1(a-c). At 433°C (a), part of a poorly-resolved semicircular arc with resistance R_1 is observed at high frequencies (schematic fit is shown, dashed, as a visual aid) and at lower frequencies, a spike. The spike becomes the high frequency tail of a second arc with resistance R_2 at higher temperatures, as shown in (b). The same data plotted as a capacitance, C' spectroscopic plot (d), show a high frequency plateau, $C_1 \sim 0.54$ pFcm^{-1}, that is attributed to the bulk response and corresponds to a relative permittivity of ~ 6.04, given by:

$$\varepsilon' = C'/\varepsilon_0 \qquad (1)$$

where ε_0 is the permittivity of free space, 8.854×10^{-14} Fcm^{-1}. Further evidence of the bulk response is given in the spectroscopic M" plot (e); this shows a Debye-like peak in the same frequency range as the poorly-resolved, high frequency arc in Z*. Because the largest peak in an M" spectrum is dominated by the component with the smallest capacitance [22], M" spectra provide a very useful, visual way to identify the bulk response of a sample.

The second arc and resistance R_2 dominates the impedance complex plane at 762°C (b); at 923 °C (c) a third, low frequency arc with resistance (extrapolated) R_3 is seen. The capacitance data at 762 °C (d) show a plateau, C_2 around 10 pFcm^{-1} at similar intermediate frequencies to the second impedance arc. At 923 ^{0}C, a low frequency dispersion in C' with values above 10 μFcm^{-1} is observed (d) at similar frequencies to the low frequency arc. From the magnitudes of their capacitances, these three impedance elements were attributed tentatively, with decreasing frequency, to the bulk effect (R_1), grain boundary

or minor second phase (R_2) and sample-electrode interface (R_3). Values for the resistances R_1 and R_2 were estimated directly from the intercepts of semicircles with the Z' axis and are shown as conductivity Arrhenius plots in (f). R_1 has activation energy 0.92(4) eV and, as discussed later, is associated primarily with bulk oxide ion conduction whereas R_2 is more resistive, with high activation energy, 2.29(2) eV, and is attributed to a grain boundary whose conductivity is mainly electronic.

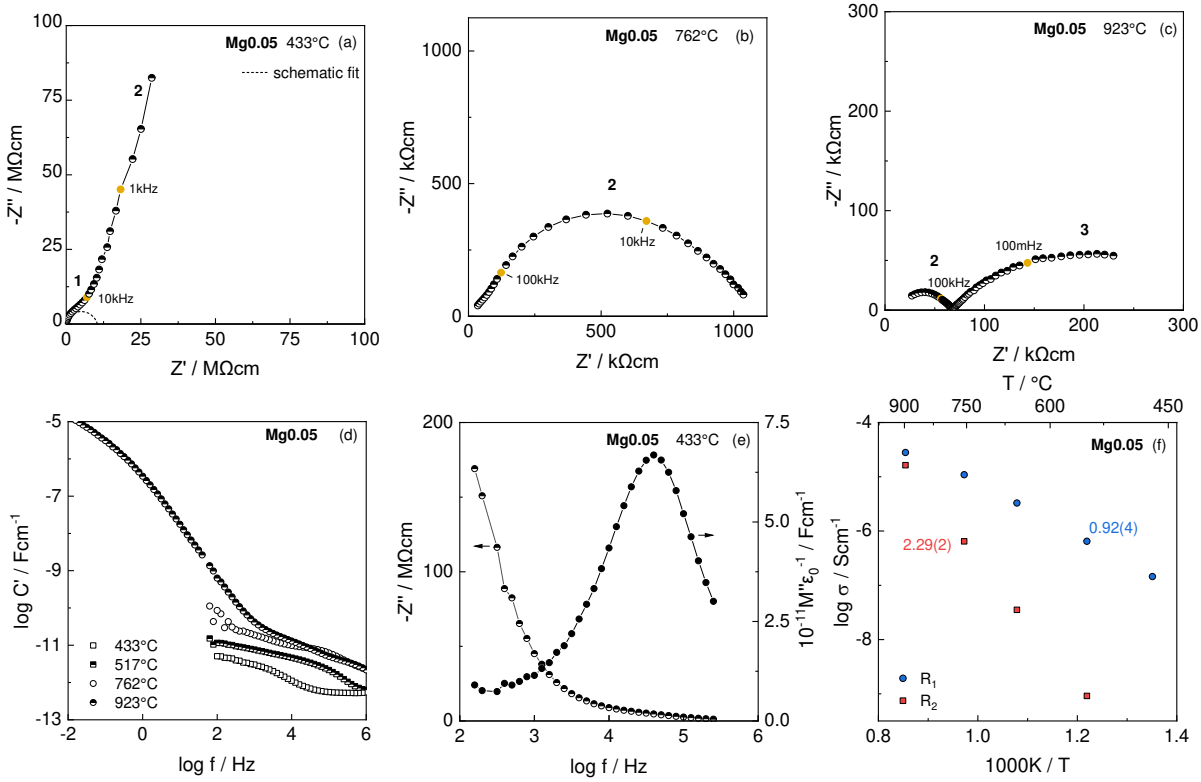

***Figure 1**. (a)-(c) Impedance complex plane plots and spectroscopic plots of (d) capacitance and (e) Z"/M" at different temperatures for Mg0.05; (f) Conductivity Arrhenius plot of bulk, R_1 and grain boundary, R_2 impedances*

Mg0.5 also gave typical impedance data sets with three electrical components, Figure 2. The impedance complex plane at 909°C (a) shows two arcs of similar size at high frequencies and a broad depressed arc at low frequencies. The C' data at this temperature (b) show, similarly, a low frequency dispersion approaching 0.62 μFcm^{-1}, an intermediate plateau around ~ 15 pFcm^{-1} and a high frequency limiting capacitance ~ 0.88 pFcm^{-1}, which is seen more clearly at lower temperature, 708°C (b) and corresponds to a bulk relative permittivity of ~ 9.9. The Z"/M" plots at 909°C, (c), show that the highest frequency Z'' peak and impedance complex plane arc (a) correspond to the component with the lowest capacitance, C_1 that is responsible for the M'' peak.

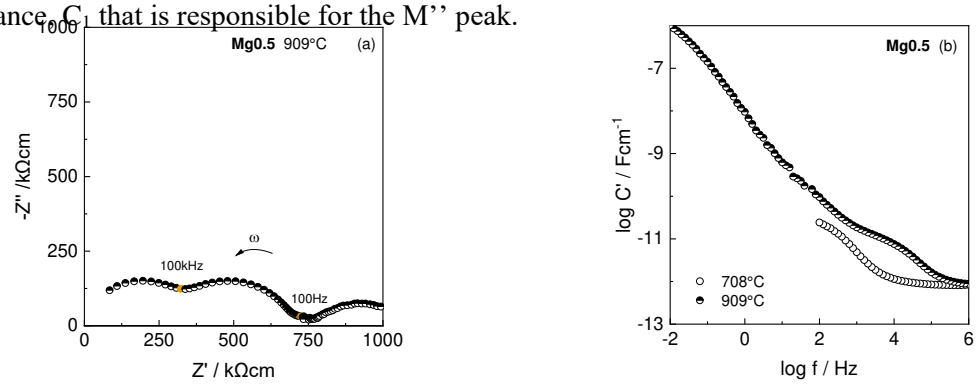

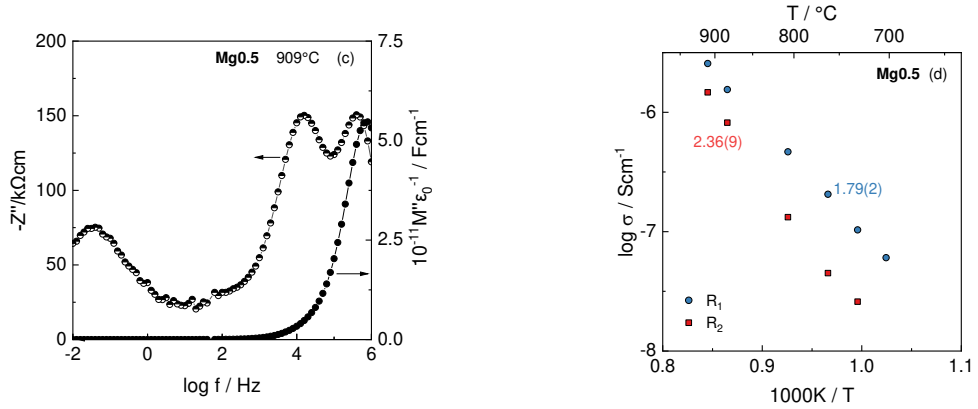

***Figure 2**. (a) Impedance complex plane plot and spectroscopic plots of (b) capacitance and (c) Z''/M'' at different temperatures for Mg0.5; (d) Conductivity Arrhenius plot of bulk, R_1 and grain boundary, R_2 impedances*

The main difference between Mg0.05 and Mg0.5 datasets is that, although both have impedance components of similar geometric dimensions from the values of C_1 and C_2, the values of resistances R_1, R_2 and R_3 are comparable for Mg0.5 whereas for Mg0.05, R_1 is relatively, much smaller than the other two resistances. Arrhenius plots for Mg0.5, Fig 2(d), show that there is not the same dramatic difference between R_1 and R_2 that is seen with Mg0.05, Fig 1(f); we attribute this difference to the reduced level of oxide ion conduction in Mg0.5, discussed later.

Arrhenius plots for both samples are collected in Figure 3 where they are separated into (a) bulk and (b) grain boundary components. The bulk conductivities, σ_1 decrease with increasing amount of dopant, in the sequence Mg0.05 > Mg0.5. However, the grain boundary conductivities, σ_2 have similar activation energy and differ by only one order of magnitude in conductivity.

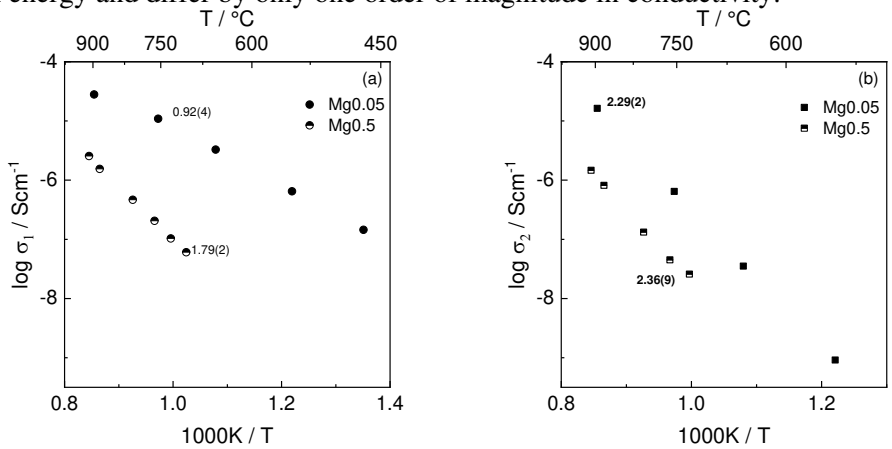

***Figure 3**. Comparison of conductivity Arrhenius plots of (a) bulk and (b)grain boundary conductivities*

Both samples showed dependence of conductivity on oxygen partial pressure, pO_2 at~900 ^{0}C, as shown in Figure 4(a-b), but not at lower temperature (c-d). In each case, at~900 ^{0}C the total resistance of the samples, as well as the three individual resistance components for both Mg0.05 and Mg0.5, decreased with increasing pO_2. This behaviour suggests a *p*-type electronic contribution to the conductivity at higher temperatures since the following idealised equilibrium at the sample surfaces is displaced to the right with increasing pO_2:

$$1/2O_2 \leftrightarrow O_o^{''} + 2h^{\bullet} \qquad (2)$$

At lower temperatures, the absence of any pO_2 dependence suggests that under these conditions (c,d), the samples are within the electrolytic domain and any *p*-type conductivity is too small to detect in the presence of the oxide ion conductivity.

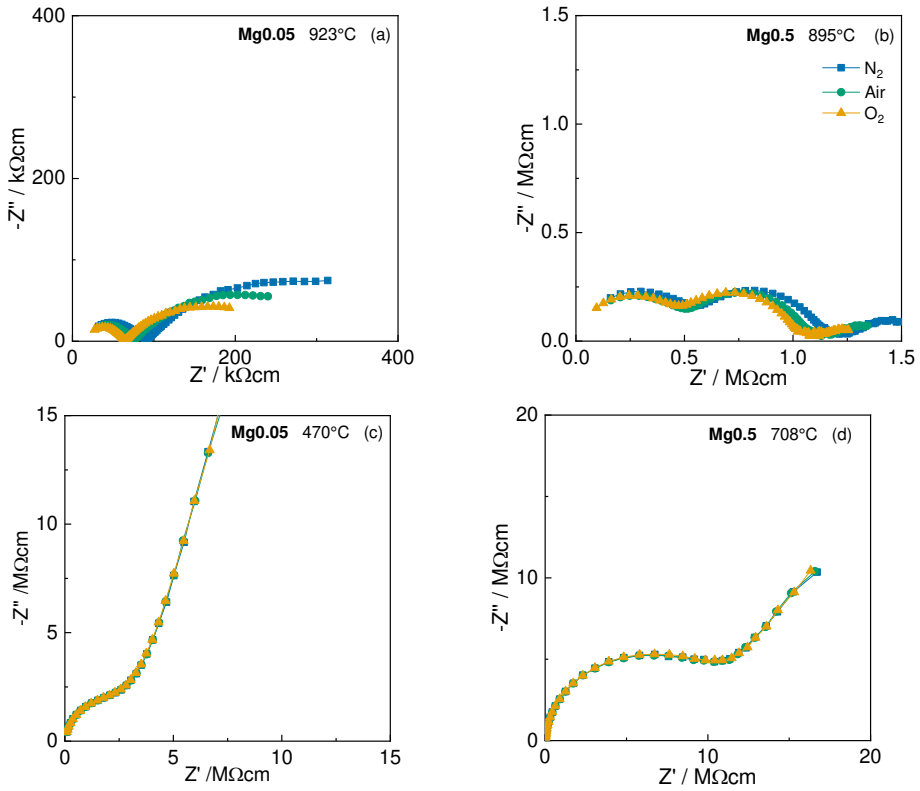

Figure 4. *Impedance complex plane plots showing pO_2-dependence of Mg0.05 and Mg0.5 at different temperatures.*

SEM/EDS results are shown in Figures 5 and 6. Secondary electron, SE, images, 5(a), for Mg0.05 show a small amount of closed porosity and grain sizes in the range 0.7-5 μm with an average of~2 μm; EDS images, 5(b,c), show a homogeneous distribution of Al and Mg. For Mg0.5, SE images, 6(a), show a wider range of grain sizes, 0.7-40 μm with an average of~15 μm and slightly more closed porosity; EDS maps, 6(b-d), show a homogeneous distribution of Al, Mg and Si through the grains with minor amounts of isolated Si segregation.

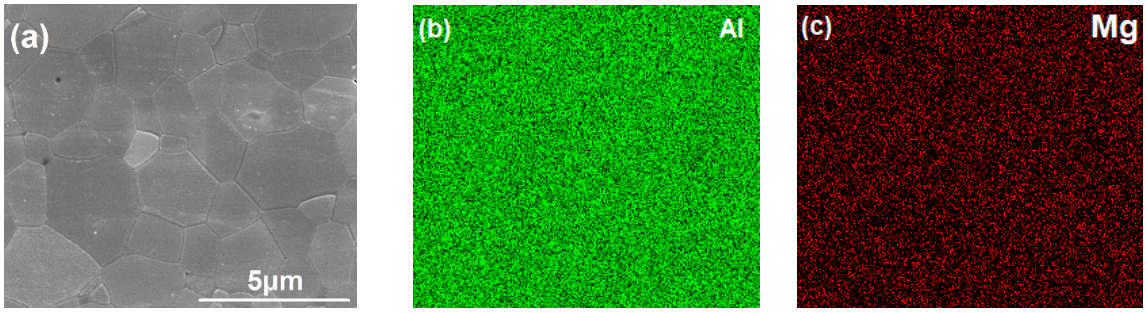

Figure 5. *(a) SE and (b,c) EDS images of polished and thermal-etched pellet of Mg0.05.*

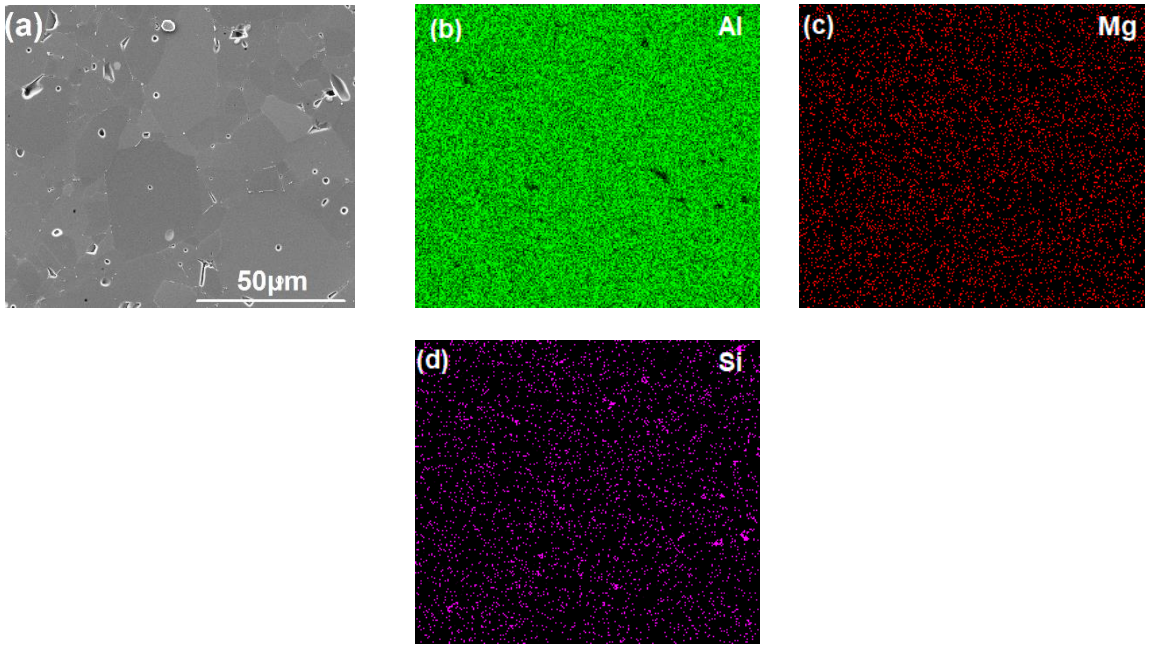

***Figure 6**. (a) SE and (b-d) EDS images of polished and thermal-etched pellet of Mg0.5.*

4.Discussion

The impedance data for both Mg0.05 and Mg0.5 show three components which indicate an equivalent circuit consisting, to a first approximation, of three parallel RC elements in series. Resistance values were obtained readily from the intercepts, or extrapolated intercepts, of arcs on the Z' axis of impedance complex plane plots. However, the impedance arcs were broadened from an ideal semi-circular shape; detailed circuit analysis and fitting would require inclusion of constant phase elements in the equivalent circuit but was not deemed necessary since resistance values were obtained directly from Z* plots. Resistance data gave linear Arrhenius plots and activation energies in the range 0.92(4) to 2.36(9) eV.

Capacitance values were estimated from plateaux in spectroscopic plots of log C'. Using the relation:

$$C = e_0\varepsilon' Ad^{-1} \qquad (3)$$

where A and d represent the area and thickness of regions responsible for a particular impedance effect, the capacitance values were assigned as follows: C_1 - sample bulk; C_2 - grain boundaries; C_3 - sample-electrode interface. Permittivity values calculated from C_1 were in the range 6-10, consistent with values expected for dielectric Al_2O_3. Values for C_2, around 10^{-11} Fcm^{-1}, indicated that the thickness of the grain boundary regions was approximately 5-10 % that of the bulk grains, assuming a simple model in which $C\alpha d^{-1}$, equation (3). It should be emphasised that these capacitance values and relative thicknesses refer to the ***electrical*** microstructure of the samples, which is not necessarily the same as the microstructure determined by direct microscopic observation. Limiting values of C_3 at 10^{-2} Hz were, for Mg0.5, $>10^{-6}$ Fcm^{-1} and for Mg0.05, $>10^{-5}$ Fcm^{-1}, which clearly correspond to the sample-electrode contact impedances.

Information on the nature of the current carriers responsible for the conductivity data was obtained from a combination of impedance measurements at different frequencies and in atmospheres of different pO_2. The results taken together indicate a temperature- and composition-dependent combination of oxide ion conduction and *p*-type electronic conduction.

Ionic conduction is indicated by a high value of sample-electrode capacitance at low frequencies: double layer capacitances of $\sim 10^{-5}$ Fcm^{-1} are typical of ion blocking at sample-electrode interfaces. Experimental values obtained here, $>3x10^{-5}$ Fcm^{-1} at 10^{-2} Hz for Mg0.05, are attributed to oxide ions as

the conducting species responsible, consistent with a charge compensation mechanism of oxygen vacancy creation on doping alumina with Mg^{2+}. For Mg0.5, the alumina appeared to be double-doped with self-compensating Mg^{2+} and Si^{4+}, which greatly reduced the need for oxygen vacancy creation; the smaller value of the capacitance, 10^{-6} Hz at 10^{-2} Hz, is consistent with a reduced level of oxide ion conductivity.

The impedance response of oxide ion conductivity may also be sensitive to pO_2 for two possible reasons. First, redox transfer of oxygen usually occurs across the sample-electrode interfaces and can be represented by a charge transfer resistance, R_{CT}, in parallel with a blocking double layer capacitance, C_{DL}. The effect of R_{CT} is to transform an 'electrode spike' into a low frequency impedance arc whose magnitude may depend on pO_2 in the surrounding atmosphere. The oxygen redox reaction, given ideally by:

$$1/2O_2 + 2e \leftrightarrow O^{2-} \qquad (4)$$

occurs in opposite directions at the two electrodes, one of which, either the oxygen evolution reaction, OER, or the oxygen reduction reaction, ORR, is likely to control the overall impedance and measured R_{CT} value.

Second, permeation of oxygen molecules, either towards or away from the sample-electrode interface may be a rate-limiting step in the overall impedance. To represent this, a Warburg impedance, Z_W, is usually placed in series with the rest of the equivalent circuit and becomes the limiting, zero frequency impedance of the measuring system. Both of these effects, R_{CT} and Z_W, may therefore make a contribution to the value of R_3. Although the electrode response, R_3C_3 of oxide ion conductors may be sensitive to pO_2, the sample resistances themselves, R_1 and R_2 do not change because the effect of pO_2 on oxide ion vacancy concentration is very small. As discussed later, a small uptake of oxygen may occur at sample surfaces and interfaces with increasing pO_2, which is compensated by the onset of *p*-type electronic conductivity, but the overall change in oxygen vacancy concentration is too small to influence the level of oxide ion conductivity.

Electronic conduction can also be studied by measurements in atmospheres of different pO_2 which in particular, can provide information concerning the nature of electronic charge carriers, as shown in the data obtained at ~900 °C, Figure 4. For materials that are conductors of oxide ions alone, as indicated above, the bulk and grain boundary conductivities should not be sensitive to pO_2. For materials that are low level electronic semiconductors, however, measurements in different pO_2 allow distinction between *n*- and *p*- type carriers. From equations (2) and (4), the effect of increasing pO_2 is either to decrease the number of *n*-type carriers (4) or to increase the number of *p*-type carriers (2). Results obtained here with both samples showed enhanced conductivity with increased pO_2 and therefore, *p*-type extrinsic conductivity. This must occur in parallel with any oxide ion conductivity and therefore, the materials are mixed conductors.

At this stage, we have no information on the relative transport numbers of holes and oxide ions, but clearly both are significant and the electronic transport numbers are not fixed but vary with pO_2. The bulk conductivity of Mg0.05 is 1-2 orders of magnitude higher than that of Mg0.5 and also has a much lower bulk activation energy, whose value, 0.92(4) eV is typical of oxide ion conductors such as yttria-stabilised zirconia, YSZ [23]. We therefore suggest that Mg0.05 is primarily an oxide ion conductor whereas Mg0.5 is primarily an electronic conductor.

In our experience of sample-electrode contacts in materials that are electronically conducting, a contact impedance is commonly observed (ie contacts may be non-ohmic) but is not double layer in nature.

Since there is no capacitive charge build-up, the interface behaves effectively as a parallel RC element in which the capacitance represents an, often poor, contact between rough surfaces of the sample and metal electrode and typically, has much smaller capacitance values. The smaller value of the low frequency capacitance for Mg0.5 compared with that for Mg0.05 is consistent with electronic conductivity but also a certain amount of oxide ion conductivity.

We consider next the possible mechanism(s) for incorporating Mg and Si dopants into the alumina samples. The SEM/EDS results give two important conclusions. First, in composition Mg0.05, the Mg is distributed homogeneously through the alumina grains with no indication of any segregation. Second, in Mg0.5, both Mg and Si are distributed homogeneously through the alumina lattice.

Mg^{2+} and Al^{3+} are similar-sized ions with similar bonding character and are able to substitute readily for each other in crystal structures, as shown by the variable stoichiometry of $MgAl_2O_4$ spinel in the MgO-Al_2O_3 phase diagram. Addition of MgO to Al_2O_3 could, in principle, involve two possible ionic charge compensation mechanisms. The general formulae that arise, as well as use of Kroger-Vink notation to describe the reactions, are as follows:

1.Creation of oxygen vacancies in $Al_{2-x}Mg_xO_{3-\frac{x}{2}}$

$$2MgO \xrightarrow{Al_2O_3} 2Mg'_{Al} + V_O^{\bullet\bullet} + 2O_O^x \qquad (5)$$

2.Creation of interstitial cations in $Al_{2-2x}Mg_{3x}O_3$:

$$3MgO \xrightarrow{Al_2O_3} 2Mg'_{Al} + Mg_i^{\bullet\bullet} + 3O_O^x \qquad (6)$$

A related possibility is that the interstitial Mg^{2+} ions may change places with lattice Al^{3+} ions to give interstitial Al^{3+} ions, consistent with a Frenkel defect model for alumina.

3.Creation of holes. An electronic charge compensation mechanism requires the creation of holes, but neither Mg^{2+} or Al^{3+} are possible as locations of holes due to their very high subsequent ionisation potentials. The observed, thermally-activated *p*-type conductivity at high temperatures and its dependence on pO_2, is therefore attributed to creation of holes on oxygen to give, $Al_{2-x}Mg_xO_{3-(x/2)+\delta}$:

$$1/2O_2 + V_o^{\bullet\bullet} + O_o^x \leftrightarrow 2O_o^{\bullet} \qquad (7)$$

In this mechanism, O_2 molecules from the surrounding atmosphere absorb on the sample surface, dissociate, pick up electrons from neighbouring under-bonded oxide ions which ionise singly and occupy oxygen vacancies as O^- ions.

In summary, only mechanism 1, equation (5), involves oxygen vacancy creation and therefore, readily accounts for the observed oxide ion conduction. Mechanism 2 could conceivably give rise to conduction by interstitial Mg^{2+} or Al^{3+} ions but not to hole conduction. Mechanism 3 accounts for hole conduction and the ready variation in *p*-type conductivity with changing pO_2, but not oxide ion conduction. Both ionic and electronic mechanisms are generally involved, therefore and the relative importance of each depends on experimental conditions, especially temperature and pO_2.

The sizes of Si^{4+} and Al^{3+} are also similar and many examples of mixed site occupancy exist in the large family of aluminosilicate minerals and their synthetic analogues. In these, Si occupies tetrahedral sites exclusively. It is rare, but not unknown, for Si to occupy octahedral sites, as in glassy and crystalline Si phosphates [24]. In Mg0.5, the SEM / EDS results support a mechanism by which Al_2O_3 is co-doped with both Mg^{2+} and Si^{4+}:

$$MgO + SiO_2 \xrightarrow{Al_2O_3} Mg_{Al}^{'} + Si_{Al}^{\bullet} + 3O_o^{x} \quad (8)$$

Further work is required to determine whether both Si and Mg occupy octahedral sites or whether Si occupies tetrahedral sites. However, a direct consequence of the co-doping mechanism, irrespective of the details concerning the location of Si, is that creation of oxygen vacancies is not necessary to compensate for equal amounts of Mg and Si dopants.

We now consider the requirements for *p*-type conductivity in the doped aluminas. Equation (7) appears to be the mechanism responsible and in particular, requires (i) the availability of oxygen vacancies to absorb oxygen with increasing pO_2 and (ii) the availability of underbonded oxide ions which can ionise readily, transferring one electron to an incoming oxygen atom and thereby generating two singly charged O^- ions. Under-bonded oxide ions may be regarded as those in the vicinity of Mg^{2+} dopant ions, also regarded as acceptor dopants, since such oxide ions are not surrounded exclusively by Al^{3+} ions and do not experience a full quota of positive charge, 2+.

The bulk conductivity of Mg0.5 is significantly lower than that of Mg0.05 although it contains 10x more Mg than Mg0.05, but nevertheless, it is still a modest mixed hole/oxide ion conductor. We find a ready explanation of this based on our results in which the concentration of both oxygen vacancies and electron holes is reduced and also in the literature on sintering and microstructural studies of doped alumina ceramics [25-27]: a key result was that the solubility of Mg in alumina is greatly enhanced by co-doping with Si. The sintering studies also showed that the initial location of dopants at grain boundaries (as expected by the in-diffusion mechanism associated with dopant incorporation) was followed by a gradual incorporation of Mg and Si into the grain interiors after, for example, heating at 1525 ^oC for 3 hours.

Literature data on well-sintered ceramics [25-27] show well-defined, thin grain boundaries, typically 1 nm thick, with segregation of dopants, at least in the early stages of sintering. Electrical microstructure results presented here on the well-sintered samples indicate that electrically, the grain boundary regions are very much thicker, even though the SE images show clear microstructures with narrow and pore-free contacts between grains. There is an apparent conflict, therefore, between the two types of microstructure, determined either directly by microscopy [25-27] or indirectly by impedance spectroscopy. Possibly, there are two types of grain boundary, thin ones seen by high resolution electron microscopy [25-27] which do not impact on the electrical properties and thick ones detected indirectly by impedance spectroscopy but for which there is no direct microscopic evidence. The grain boundary regions seen in the impedance data are more resistive than the bulk regions; they have higher activation energy and therefore, the concentration of mobile oxygen vacancies is less. The EDS results do not show any significant variation in Mg distribution throughout the grains. Possibly, a different mechanism of charge compensation exists in the grain boundary regions, such as the creation of either interstitial Mg^{2+} ions, equation (6), or O^- ions, equation (7) both of which avoid the creation of oxygen vacancies. Further studies, including high resolution TEM would be required to determine whether there is any cation segregation at the thin grain boundaries; from the impedance results, however, there is no evidence of any additional impedance associated with thin grain boundary regions.

The results reported here, showing high temperature conductivity properties that range from oxide ion conduction to *p*-type electronic conduction, depending on composition, pO_2 and temperature, are consistent with early measurements on the *dc* conductivity of pure and Mg-doped alumina single crystals and polycrystals [6], [10]. Direct comparison with the literature is difficult, however, since our *ac* results show that grain boundary resistances dominate the impedance at lower temperatures whereas the higher activation energy of grain boundary resistances means that bulk resistances may dominate their impedance at temperatures ≥ 900°C, beyond the present measuring range and assuming linear Arrhenius behaviour.

Nevertheless, it is clear from [6], [10] that the materials are essentially *p*-type conductors at high temperature and increasingly, show a broad, pO_2-dependent electrolytic domain with ionic conductivity at lower temperatures. The general behaviour of Mg-doped polycrystalline Al_2O_3 [6] was reported to be similar to that of single crystal samples but the transition to electronic conduction occurred at lower temperatures and lower pO_2; possibly, this was because the higher oxygen vacancy concentration in the samples promoted an increase in *p*-type conduction. The activation energies for conductivity reported in [6] were in the range 2.5 to 3.5 eV; these are not inconsistent with our grain boundary activation energies in the range 2.29-2.36 eV. Our much lower bulk activation energy of 0.92 eV for Mg0.05 would not have been observed in *dc* measurements because of (i) the high grain boundary activation energy at lower temperatures and (ii) a switch to electronic conductivity at high temperatures.

We are unable to resolve the conundrum of the discrepancy between experimental and calculated diffusion parameters highlighted in [2]–[4], but are able to suggest some additional factors that may merit consideration. From our results and the early literature on electrical properties, it is clear that for conductivity measurements in air or O_2, of both nominally pure and doped Al_2O_3, the materials are mixed conductors ranging from mainly oxide ion conduction at lower temperatures to *p*-type semi-conduction at the high temperatures, ~1600 °C, that are typically used in diffusion measurements. The *p*-type conductivity is likely to be a hopping conductivity which means that the holes are localised on an atomic species, for which the only realistic possibility is oxygen. Holes on oxygen equate to lower valence O^- ions instead of the ubiquitous O^{2-} ions. The structures therefore contain mixed anions, O^- and O^{2-}, as well as showing mixed ionic and electronic conductivity. Since O^- ions and the associated holes appear to be the dominant defects that control conductivity at 1600°C, their role in diffusion processes, of both Al and O, may be significant.

We show clear evidence for two ionic charge compensation mechanisms, leading to either oxygen vacancies or self-compensation of aliovalent cations, with the possibility under certain circumstances of a third mechanism involving either interstitial Mg^{2+} ions or O^- ions that fill available oxygen vacancies. Each of these compensation mechanisms may impact differently on the measurement of diffusion coefficients.

5. Conclusions

Some general conclusions can be drawn concerning the electrical properties of alumina ceramics, based on samples prepared with different doping schedules that were studied here.

The main charge compensation mechanism for incorporation of Mg^{2+} ions as a single dopant into the alumina lattice appears to involve oxygen vacancy creation. This is responsible for the observed oxide ion conduction, for which evidence is provided by the presence of double layer capacitance effects in low frequency impedance data.

In the presence of Si, literature data suggest that dissolution of Mg is enhanced by a double substitution mechanism in which charge balance is achieved without oxygen vacancy creation. This is confirmed by our EDS results showing a uniform distribution of both Mg and Si dopants through the alumina grains and accounts for the much reduced oxide ion conductivity associated with a reduced oxygen vacancy concentration observed in composition Mg0.5 compared with Mg0.05.

The Mg-doped samples are mixed conductors of both oxide ions and holes. The level of hole conductivity is sensitive to oxygen partial pressure in the surrounding atmosphere. This sensitivity indicates rapid oxygen exchange between the surrounding atmosphere and sample surfaces at ~900 ^{o}C and is probably facilitated by the presence of oxygen vacancies in Mg-doped alumina.

The easy creation of holes on oxygen, as O^- ions, is attributed to the under-bonding of certain oxide ions associated with the acceptor dopant Mg^{2+}. Absorption of O_2 molecules and creation of holes may be represented ideally by equation (2), similar to what was proposed to account for the occurrence of *p*-type conductivity in acceptor-doped Ba and Sr titanate perovskites [28].

Although Al_2O_3 is regarded as a 'classic' ionic oxide, at high temperatures it is a *p*-type electronic semiconductor with holes located on oxygen. This means that, to achieve charge balance of O^- ions, a slight excess of oxygen, beyond that of the Al_2O_3 stoichiometry, may be required and especially, be facilitated by the availability of oxygen vacancies in Mg-doped alumina. In contrast to ceramic oxides such as TiO_2 and $BaTiO_3$, that lose a small amount of oxygen at high temperature by oxidation of some near-surface lattice O^{2-} ions and exhibit *n*-type semiconductivity, Mg-doped alumina shows only partial oxidation of O^{2-} ions, by reaction with O_2, giving rise to *p*-type semiconductivity associated with the resulting O^- ions.

Acknowledgements

JRG thanks CONACyT for a studentship, grant number 578893. Ian Ross (Sorby Centre, University of Sheffield) is acknowledged for significant help with the EM measurements.

References

[1] Y. Oishi and W. D. Kingery, "Self-Diffusion of Oxygen in Single Crystal and Polycrystalline Aluminum Oxide," *J. Chem. Phys.*, vol. 33, pp. 480–486, 1960, doi: 10.1063/1.1731170.

[2] A. H. Heuer and K. P. D. Lagerlof, "Oxygen self-diffusion in corundum (α-Al_2O_3): A conundrum," *Philos. Mag. Lett.*, vol. 79, no. 8, pp. 619–627, 1999, doi: 10.1080/095008399177002.

[3] A. H. Heuer, "Oxygen and aluminum diffusion in α-Al_2O_3: How much do we really understand?," *J. Eur. Ceram. Soc.*, vol. 28, no. 7, pp. 1495–1507, 2008, doi: 10.1016/j.jeurceramsoc.2007.12.020.

[4] J. H. Harding, K. J. W. Atkinson, and R. W. Grimes, "Experiment and Theory of Diffusion in Alumina," *J. Am. Ceram. Soc.*, vol. 86, no. 4, pp. 554–59, Apr. 2003, doi: 10.1111/j.1151-2916.2003.tb03340.x.

[5] J. Pappis and W. D. Kingery, "Electrical Properties of Single-Crystal and Polycrystalline Alumina at High Temperatures," *J. Am. Ceram. Soc.*, vol. 44, no. 9, pp. 459–464, Sep. 1961, doi: 10.1111/j.1151-2916.1961.tb13756.x.

[6] N. M. Tallan and H. C. Graham, "Interfacial Polarization and Electrical Conductivity in Sapphire," *J. Am. Ceram. Soc.*, vol. 48, no. 10, pp. 512–516, 1965.

[7] K. J. W. Atkinson, R. W. Grimes, M. R. Levy, Z. L. Coull, and T. English, "Accommodation of impurities in α-Al_2O_3, α-Cr_2O_3 and α-Fe_2O_3," *J. Eur. Ceram. Soc.*,

vol. 23, no. 16, pp. 3059–3070, 2003, doi: 10.1016/S0955-2219(03)00101-8.
[8] J. Pan, J. Öijerholm, A. B. Belonoshko, A. Rosengren, and C. Leygraf, "Self-diffusion activation energies in α-Al_2O_3 below 1000°C - Measurements and molecular dynamics calculation," *Philos. Mag. Lett.*, vol. 84, no. 12, pp. 781–789, 2004, doi: 10.1080/09500830500071051.
[9] J. Öijerholm, "Ionic transport of α -alumina below 1000 ° C An in-situ impedance spectroscopy study," RoyalInstitute of Technology, Stockholm, Sweden, 2004.
[10] R. J. Brook, J. Yee, and F. A. Kröger, "Electrochemical Cells and Electrical Conduction of Pure and Doped Al_2O_3," *J. Am. Ceram. Soc.*, vol. 54, no. 9, pp. 444–451, 1971, doi: 10.1111/j.1151-2916.1971.tb12382.x.
[11] K. Kitazawa and R. L. Coble, "Electrical Conduction in Single-Crystal and Polycrystalline Al_2O_3 at High Temperatures," *J. Am. Ceram. Soc.*, vol. 57, no. 6, pp. 245–250, 1974, doi: 10.1111/j.1151-2916.1974.tb10879.x.
[12] H. P. R. Frederikse and W. R. Holser, *High Temperature Electrical Conductivity of Aluminum Oxide*, vol. 9. Boston, 1975.
[13] S. K. Mohapatra and F. A. Kröger, "Defect Structure of α-Al_2O_3 Doped with Magnesium," *J. Am. Ceram. Soc.*, vol. 60, no. 3–4, pp. 141–148, 1977, doi: 10.1111/j.1151-2916.1977.tb15490.x.
[14] H. A. Wang and F. A. Kröger, "Chemical Diffusion in Polycrystalline Al_2O_3," *J. Am. Ceram. Soc.*, vol. 63, no. 11–12, pp. 613–619, Nov. 1980, doi: 10.1111/j.1151-2916.1980.tb09846.x.
[15] D. S. Phillips, T. E. Mitchell, and A. H. Heuer, "Precipitation in star sapphire III. Chemical effects accompanying precipitation," *Philos. Mag. A Phys. Condens. Matter, Struct. Defects Mech. Prop.*, vol. 42, no. 3, pp. 417–432, 1980, doi: 10.1080/01418618008239367.
[16] P. W. M. Jacobs and E. A. Kotomin, "Defect energies for pure corundum and for corundum doped with transition metal ions," *Philos. Mag. A Phys. Condens. Matter, Struct. Defects Mech. Prop.*, vol. 68, no. 4, pp. 695–709, 1993, doi: 10.1080/01418619308213992.
[17] K. P. D. Lagerlöf and R. W. Grimes, "The defect chemistry of sapphire (α-Al_2O_3)," *Acta Mater.*, vol. 46, no. 16, pp. 5689–5700, Oct. 1998, doi: 10.1016/S1359-6454(98)00256-0.
[18] A. J. Ruys, *Alumina Ceramics: Biomedical and Clinical Applications*. Woodhead Publishing, 2018.
[19] R. L. Coble, "Sintering Crystalline Solids. II. Experimental Test of Diffusion Models in Powder Compacts," *J. Appl. Phys.*, vol. 32, no. 5, pp. 793–799, 1961, doi: 10.1063/1.1736108.
[20] S. J. Bennison and M. P. Harmer, "Effect of MgO Solute on the Kinetics of Grain Growth in $A1_2O_3$," *J. Am. Ceram. Soc.*, vol. 66, no. 5, p. C-90-C-92, 1983, doi: 10.1111/j.1151-2916.1983.tb10065.x.
[21] R. M. German, P. Suri, and S. J. Park, "Review: liquid phase sintering," *J. Mater. Sci.*, vol. 44, no. 1, pp. 1–39, 2009, doi: 10.1007/s10853-008-3008-0.
[22] D. P. Almond and A. R. West, "Impedance and modulus spectroscopy of 'real' dispersive conductors," *Solid State Ionics*, vol. 11, no. 1, pp. 57–64, 1983, doi: 10.1016/0167-2738(83)90063-2.
[23] X. Vendrell and A. R. West, "Electrical Properties of Yttria-Stabilized Zirconia, YSZ Single Crystal: Local AC and Long Range DC Conduction," *J. Electrochem. Soc.*, vol. 165, no. 11, pp. F966–F975, 2018, doi: 10.1149/2.0881811jes.
[24] T. Weeding, B. de Jong, W. Veeman, et al. "Silicon coordination changes from 4-fold to 6-fold on devitrification of silicon phosphate glass," *Nature* ,vol 318, pp 352–353, 1985, doi: 10.1038/318352a0
[25] C.A. Handwerker, P.A. Morris and R.L. Coble, "Effects of chemical inhomogeneities on grain growth and microstructure in Al_2O_3," *J. Am. Ceram. Soc.*, vol 72, pp130-136, 1989
[26] T. Frueh, C. Marker, E.R. Kupp, C. Compson, J. Atria, J.L. Gray, Z-K. Liu and G.L. Messing, "Powder chemistry effects on the sintering of MgO-doped specialty Al_2O_3," *J. Am. Ceram. Soc.*, vol 101, pp2739-2751, 2018
[27] K.L. Garilov, S.J. Bennison, K.R. Mikeska, J.M. Chabala and R. Levi-Setti, "Silica and

magnesia dopant distributionsin alumina by high resolution scanning secondary ion mass spectrometry," *J. Am. Ceram. Soc.*, vol 82, pp 1001-1008, 1999

[28] M. Guo, N. Maso, Y. Liu, and A. R. West, "Electrical Properties and Oxygen Stoichiometry of Ba_{1-x} Sr_x $TiO_{3-\delta}$ Ceramics," *Inorg. Chem.*, vol. 57, pp. 64–71, 2018, doi: 10.1021/acs.inorgchem.7b01827.